JJBS

Volume 17, Number 4,December 2024
ISSN 1995-6673
Pages 615 – 725
https://doi.org/10.54319/jjbs/170414

Jordan Journal of Biological Sciences

The C-terminal Domain of S1 Subunit Spike Protein Enhances the Sensitivity of COVID-19 Serological Assay

Sabar Pambudi[1,4,*], Nihayatul Karimah[1], Ika Nurlaila[1], Doddy Irawan[1], Tika Widayanti[1], Jodi Suryanggono[1], Asri Sulfianti[1], Sjaikhurrizal El Muttaqien[1], Vivi Setiawaty[2], Hana Pattipeiluhu[3], Muhammad Luqman[1]

[1]*Research Center for Vaccine and Drug, National Research and Innovation Agency (BRIN), Tangerang Selatan, 15310, Indonesia;* [2]*Ministry of Health, Jakarta, 10560, Indonesia;* [3]*Moh Ridwan Meureksa Hospital, Jln Taman Mini 1, Jakarta, 13560, Indonesia;* [4]*Department of Biotechnology, Universitas Esa Unggul, Jl, Arjuna Utara no.9, Jakarta, 11510, Indonesia*

Received: May 2, 2024; Revised: July 31, 2024; Accepted: August 7, 2024

Abstract

Evaluating antibody responses against the receptor binding domain (RBD) protein will be essential for determining the antibody response's durability and defining a vaccine-induced antibody response. Consequently, it becomes crucial for the production of innovative RBD antigens to enhance the sensitivity detection of antibody anti-COVID-19. The bottleneck to achieving these targets is the availability of effective RBD antigens construct. This study evaluated the potency RS1, RBD with C-terminal domain (CTD) of Spike S1 domain, to detect antibody anti-spike SARS-CoV-2 in patient sera. Docking simulations with ClusPro have been done to determine how antigens (RBD/RS1) and antibody (Fv) models interact. The RMSD for both complexes is accordingly still in tolerable value. The constructs RBD and RS1 were expressed in *Escherichia coli* strain Origami under the pET-32b(+) expression vector. The indirect IgG-ELISA of both recombinant proteins could differentiate the presence of negative antibody anti-spike in naïve sera and positive sera collected from COVID-19 patients between 2020 and 2022. Furthermore, the degree of detecting antibodies anti-spike utilizing the RS1 protein increased significantly compared to RBD (p = 0.0033). Our results indicate additional CTD in RS1 could access more anti-spike antibodies and enhance the sensitivity detection of antibody anti-spike COVID-19.

Keywords: COVID-19, C-terminal domain, Receptor Binding Domain, Serological assay

1. Introduction

The emerging of SARS-CoV-2 in Wuhan-China initiated the COVID-19 pandemic with a notable global mortality rate (Oglat *et al.*, 2022; Rastogi *et al.*, 2020). The spike (S), membrane (M), envelope (E), and nucleocapsid (N) are the structural proteins of the SARS-CoV-2 virus. The spike protein contains 1273 amino acid residues and is composed of three subunits: S1, S2, and a transmembrane (TM) domain. The N-terminal domain (NTD), receptor binding domain (RBD), and C-terminal domain (CTD) are present within the S1 subunit (Biswas *et al.*, 2021; Shwan *et al.*, 2022). The RBD attaches to the ACE2 receptor on the cell surface, facilitates the fusion of the virus and cellular membrane, and serves as an antigen to stimulate the production of antibodies that disrupt the binding between the virus and the host (Biswas *et al.*, 2021; Tai *et al.*, 2020).

The sera of the vast majority of COVID-19 survivors exhibit a telling presence of IgM and IgG antibodies directed against the SARS-CoV-2 spike protein. In order to effectively prevent and contain the spread of the virus, it is essential to meticulously track the antibody responses in patients who have either recovered from infection or received vaccination. The neutralizing antibody titer in sera serves as a vital indicator of the immunological outcome, providing valuable insights into the efficacy of the immune system's response to SARS-CoV-2 (Peterhoff *et al.*, 2021; Yin *et al.*, 2021).

The SARS-CoV-2 RBD protein is frequently employed in serological assays, commonly in ELISA-based assay platforms. These assays serve an important role in establishing past exposure to SARS-CoV-2 and analyzing vaccination efficacy in populations. Mutations in the RBD have been found to impact antibody binding and neutralization, with some variants showing different antibody responses compared to the wild type (Fraser *et al.*, 2022). The global serological test for COVID-19 is based on the RBD SARS-CoV-2 expressed in E. *coli*. Nonetheless, a previous study reported that the detection sensitivity using RBD from E. *coli* is less sensitive compared to RBD expressed in the mammalian expression system (Ayón-Núñez *et al.*, 2022). Despite the significant advances made in recent years, the RBD's production in eukaryotic systems has been hindered by two major constraints: a limited capacity to generate sufficient quantities and an exorbitant cost. These obstacles have far-reaching implications, as they undermine the potential for RBD-based medicines and vaccines to become viable

* Corresponding author. e-mail: saba002@brin.go.id; sabar.pambudi@esaunggul.ac.id.

options for treatment and prevention. The reality is that the current production limitations and prohibitively high expenses severely curtail the prospect of leveraging RBD as a valuable resource in the development of novel therapeutic agents. As a result, it is essential to address these challenges and find innovative solutions to overcome them, thereby paving the way for the widespread application of RBD-based technologies (He *et al.*, 2021).

In an effort to optimize the performance of serological assays reliant on RBD produced in E. *coli*, we have designed a novel construct, RS1, which incorporates the C-terminal domain (CTD) of the S1 spike protein. This domain's CTD exhibits a more extensive amino acid sequence compared to its SARS-CoV counterpart, thereby expanding its surface area and enhancing the interaction between SARS-CoV-2 and the ACE-2 receptor. This structural modification is anticipated to significantly boost the sensitivity of serological assays, allowing for more accurate and reliable detection of SARS-CoV-2 antibodies (Huang *et al.*, 2020). Several studies have demonstrated that the surface area of an antigen exerts a profound impact on the human immune response. The extent to which an antigen presents itself to the immune system has been shown to influence the magnitude and quality of the response (Heida *et al.*, 2022; Zinkhan *et al.*, 2021) and possibly to enhance the detection of anti-spike antibodies corresponding to COVID-19 infection.

Our data demonstrated that recombinant RBD and RS1 can be probed by rabbit monoclonal antibodies anti-RBD/Spike. Interestingly, compared to recombinant RBD, recombinant RS1 significantly increased the sensitivity of the ELISA assay from positive serum patients of COVID-19 collected from 2020 to 2022. In parallel, a computational approach was carried out to evaluate the structural interaction between RBD and RS1 against COVA2-39 which has been reported to target the RBD of SARS-CoV-2 (Wu *et al.*, 2020). COVA2-39 is a crystal structures of IGHV3-53 antibody that frequently bind SARS-CoV-2 RBD. This antibody is derived from a convalescent donor from Amsterdam and potently neutralizes SARS-CoV-2 virus (Brouwer *et al.*, 2020). In this study, this crystal structure is used as a neutralizing antibody model and to explore its interaction with RBD or RS1.

2. Materials and Methods

2.1. Samples

All samples, such as sera and RNA, from confirmed acute COVID-19 patients, were collected from 2020 to 2022 in a cohort study after approval of the Ethical Board of the NIHRD, Ministry of Health (LB.02.01/2/KE.432/2020). The antigenicity evaluation of the SARS-CoV-2 recombinant RBD and RS1 was performed using a random selection of collected sera.

2.2. Plasmid Construction

The amplification of the RBD (amino acid 319–541) and RS1 (amino acid 319–681) fragment genes of SARS-CoV-2 was carried out by PCR using Phusion Green Hot Start II High-Fidelity PCR Master Mix (Thermo) and specific primers (Fw: 5'-TAATggtaccATGAGAGTCCAACCAACAGAATCTAT TGTTAGATTTCC-3'; Rv:5'-TAATctcgagaaGGAAATTGACACATTTGTTTTTAACC AAATTAGTAGAC-3') and cloned into the pET-32b(+) bacterial expression vector with N and C-terminal His-tag. The genes were amplified with denaturation steps at 98^{o}C for 15 seconds, annealing at 60^{o}C for 15 seconds, and extension at 72^{o}C for 30 seconds. Both gene fragments and vector pET-32b(+) were double-digested with *Kpn1* and *Xho1* restriction enzymes, followed by ligation. The E. *coli* TOP10 colonies from the transformation were extracted, and the recombinant plasmids were verified by restriction enzymes and sequencing using T7 primers.

2.3. In Silico Study

The antibody used in this molecular modelling is a IGHV3-53 neutralizing antibody, COVA2-39, that reportedly can bind to RBD SARS-CoV-2 (Wu *et al.*, 2020). The PDB file of the antibody was retrieved from RCSB PDB; PDB ID: 7JMP. The structure of this antibody in PDB was in neutralizing condition with SARS-CoV-2 RBD. The variable light chain (VL) and variable heavy chain (VH) of the fragment antigen binding (Fab) were split up from the original 3D structure as variable fragment (Fv) and saved into separate PDB file. The processes of adding hydrogen atom and solvent deletion were done using YASARA software (Krieger *et al.*, 2014). The antigen structures to be modelled are the RBD and RS1 of SARS-CoV-2 and which both are fused with TrxA fusion protein from pET32b plasmid. The fusion form of TrxA protein and the antigen structures were modelled using I-TASSER server for iterative threading assembly (J. Yang *et al.*, 2015).

To obtain molecular complex of antigen-antibody, we performed docking between VH-VL structure and antigen-TrxA fusion protein structures using ClusPro (Kozakov *et al.*, 2017). ClusPro is a fast Fourier transform (FFT) algorithm-based docking server which incorporates Decoys as the Reference State (DARS) into PIPER docking program in the server for antigen-antibody complex prediction (Brenke *et al.*, 2012). An antibody mode, which set antibody as receptor and antigen as ligand, and automatic masking of non-complement determining region were chosen. The complexes of antigen-antibody resulted from docking simulation were then analyzed for visualization using YASARA in order to choose the complex that closely resembles the structure of RBD and the VH-VL of COVA2-39 antibody in the PDB ID 7JMP. It was also done by structural comparison of multiple-chain protein complexes between two structures with MM-align program (Mukherjee *et al.*, 2009).

For each chosen complex predicted by docking simulation, molecular dynamics with GROMACS 2021.5 was performed to get the insight of the dynamic interaction between VH-VL structure and antigen-TrxA fusion protein (Liu *et al.*, 2023). The pdb2gmx generated topology file for the protein complex using CHARMM36 force field and TIP3P original water model (Lee *et al.*, 2016). A rhombic dodecahedral shape defined the unit cell of the solvent environment with the protein complex in the center of 10 Å from the edge. The system was set in neutral condition with the addition of Na+ and Cl-. The steepest descent minimization of 50000 steps was done to remove bad contact with maximum force 1000 kJ.mol^{-1}.nm^{-1}. Two phases of equilibration including isothermal-isochoric ensemble (NVT) and isothermal-isobaric ensemble (NPT)

were performed with position restraint for the protein complex and LINCS constraint algorithm for the hydrogen bonds. The system was heated from 0 to 300 K with 2-fs time step for 50 ps in each equilibration phase. The forces of Van der Waals interactions were smoothly switched to zero between 10 Å and 12 Å. Particle Mesh Ewald for long-range electrostatics was applied with fourth-order (cubic) interpolation and grid spacing for FFT of maximum 0.16 nm. The temperature coupling used velocity rescaling in both NVT and NPT with time constant of 0.1 ps and reference temperature of 300 K. The pressure coupling used Berendsen method for NPT equilibration phase with 2 ps time constant, reference pressure of 1 bar, and isothermal compressibility of $4.5x10^{-5}$ bar^{-1}. The production phase of MD simulation was carried out in 50 ns with a time step of 2 fs without position restraint. The hydrogen bonds were constrained with SHAKE algorithm. The long-range electrostatics and temperature coupling was calculated the same as in equilibration phase, while the pressure coupling used Parrinello-Rahman barostat. The root mean square deviation (RMSD) of protein backbone and the root mean square fluctuation (RMSF) of residue position were computed. Residue interaction network before and after MD simulation were defined using The RING web server (Piovesan *et al.*, 2016).

2.4. Expression

The recombinant plasmids were transformed into E. *coli* Origami strains and cultivated in Luria Bertani (LB) medium containing 70 µg/ml ampicillin, 15 µg/ml kanamycin, and 12.5 µg/ml tetracycline. The positive clones were verified by PCR using a set of T7 primers. Recombinant E. *coli* with pET-32b(+)-RBD/RS1 or wild-type pET-32b(+) were cultivated until the optical density (OD) at 600 nm reached 0.8-1.0 and induced by IPTG to the final concentration of 0.3mM. The low-temperature induction was carried out at 25^{o}C, 150 rpm for 16 hours. The induced cells were harvested by centrifugation and stored at -20^{o}C for further analysis.

2.5. Isolation of inclusion bodies

The recombinant E. *coli* pellet was resuspended in PBS pH 7.4 and sonicated for 10 minutes on ice. The lysate was separated by centrifugation at 4^{o}C, 11,000 rpm for 3 min. The supernatant was removed, and the pellet was resuspended and incubated for 1 hour at room temperature with 0.1M Tris-Cl pH 8.5 or pH 11 with a variation in urea concentration. The supernatant containing inclusion bodies of recombinant RBD and RS1 proteins were separated from the pellet by centrifugation. Confirmation of the isolation of inclusion bodies was carried out by SDS-PAGE and western blot analysis.

2.6. Western Blot

All recombinant proteins were transferred onto PVDF membranes, blocked with 5% skim milk in PBST (PBS, 0.1% Tween-20), and probed with mouse anti-His monoclonal antibody (MA1-21315, Invitrogen), rabbit anti-RBD polyclonal antibody (PA5-114451, Invitrogen), and human anti-spike monoclonal antibody (MA5-35950, Invitrogen) at 4^{o}C for overnight. After washing with PBST, the IRDye 800 CW conjugated goat anti-mouse IgG antibody (1:5000) or goat anti-rabbit IgG (1:5000) or goat anti-human IgG (1:10000) was used as the secondary antibody. The membranes were washed with PBST and the signals were captured under the near-infrared optical imaging system (Odyssey Clx, LI-COR). The data was further analyzed by Image Studio ver 5.2 software.

2.7. Purification of RBD protein

The supernatants containing inclusion bodies of recombinant RBD and RS1 in 0.1M Tris-Cl pH 11 containing 2M urea were used in the purification step. The HisTrap HP column (Cytiva) was equilibrated with two-column volumes (CVs) of 20 mM phosphate buffer pH 7.4 with 300 mM NaCl and 20 mM imidazole (buffer A). The Akta Start (Cytiva) was set at a flow rate of 0.5 ml/min for loading samples into the resin and 1 ml/min for capturing, washing, and elution steps. The resin was washed with 5 CVs of buffer A followed by elution with 2 CVs of buffer B (20 mM phosphate buffer pH 7.4 with 300 mM NaCl and 250 mM imidazole. The eluted fraction was kept at 4^{o}C until further analysis.

2.8. . Indirect IgG-ELISA and statistic analysis

The indirect IgG-ELISA protocol was adapted from (Krähling *et al.*, 2021). The coating step was performed by diluting the RBD or RS1 protein with 0.1 M sodium carbonate pH 9.0 up to 100 ng in each well of the 96-well plate overnight and blocked with PBST with 10 % skim milk. The primary antibody, a 1:50 dilution of patient sera in PBST with 10% skim milk, was added to the plates for one hour. Followed by incubation with secondary antibody HRP-conjugated goat anti-human IgG (Invitrogen, 31410) for 30 minutes. The reactivity was measured with the HTX Sinergy plate reader (BIOTEK) at 450 nm after the addition of TMB substrate to the plates. Statistical significance of the differences between triplicate mean values between RBD and RS1 was determined by using a paired t-test with the software GraphPad Prism 5 (GraphPad Software, Inc, San Diego, CA, USA). The significance is indicated by asterisk (*) symbols. A positive sample is defined as having OD450 values of three standard deviations (SD) above the mean (Ayón-Núñez *et al.*, 2022) of a panel of six negative controls from naïve pre-pandemic sera.

3. Results

3.1. Plasmid Construction

The RBD fragment (319–541aa) and RS1 fragment (319–681) were obtained using the designed primers in a polymerase chain reaction (PCR). The cDNA from RNA SARS-CoV-2 isolated from a COVID-19 patient from 2020 was used as a PCR template. SnapGene generated the schematic diagram illustrating the design of the intended recombinant plasmid (Figure 1A). Double digestion with *Kpn1* and *Xho1* was carried out to check the recombinant plasmids of pET-32b(+)-RBD and pET-32b(+)-RS1 (Figure 1B). The specific band around 5,900 bp, which corresponds to the backbone of pET-32b(+), appears clearly for both constructs. The digested recombinant plasmid clearly shows the bands for RBD with a correct size of around 670 bp and RS1 with 1090 bp. The target genes were amplified by PCR using the T7 universal primer (Figure 1C), and DNA sequencing was further employed to verify the identity of the genes (data not shown).

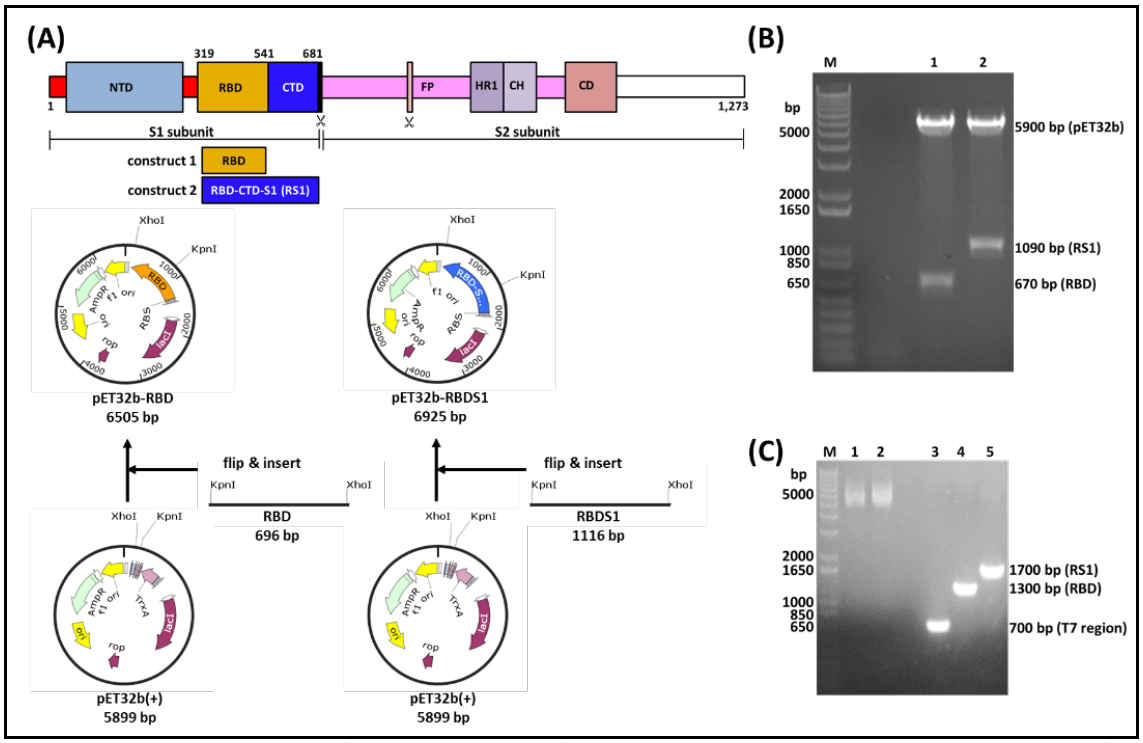

Figure 1. Recombinant plasmid verification. (A) Diagram of plasmid pET-32b(+)-RBD and pET-32b(+)-RS1. (B) Confirmation of recombinant plasmids by double digestion with *Kpn1* and *Xho1*. Both constructs showed correct fragments of insert genes and the backbone of the vector pET-32b(+) after digestion. (C) The PCR using a universal T7 primer was carried out to confirm the recombinant plasmid. Lane 1,2 are template plasmids. Lane 3 is wildtype pET-32b(+), and lane 4,5 corresponds to RBD and RS1, respectively.

3.2. In Silico Study

The fusion form of pET32b peptide "TrxA fusion protein" and the antigen structures (RBD and RS1) has been modelled. Due to the existence of TrxA fusion protein that covalently binds to the antigens, an iterative threading assembly with I-Tasser was used to build the 3D structures. The structure with the highest C-score was chosen for following simulations. C-score is the confidence score to estimate the quality of predicted structure in which the higher value indicates higher confidence of the structure quality (Yang *et al.*, 2015). The result came out that the structure of RS1 fusion form (C score = -2.39) is slightly better than the structure of RBD fusion form (C score = -3.62). No predicted structures have positive C score because the exact template for fusion form of TrxA protein and RBD/RS1 is not available. The lack of exact template also causes lower TM score (0.3 - 0.4) for each model. TM-score is a measure for assessing the topological similarity of protein structures. The value is between 0 and 1, where 1 indicates a perfect match between two structures. Correct topology can be achieved if the TM score is more than 0.5 (Xu *et al.*, 2010). Therefore, the generated topology of the models is not exactly correct but not in a random form as well.

To obtain a complex between antigen (RBD/RS1) and antibody (Fv), docking simulation with ClusPro has been performed (Figure 2). It generated 30 clusters that contain several neighboring structures within 9 Å IRMSD radius from the center structure (Kozakov *et al.*, 2017). The center structures in the five most populated clusters were then aligned with the reference complex structure (PDB ID: 7JMP) with MM-Align program to calculate sequence identity, TM-score, and RMSD. Regardless of the lowest energy in the cluster, the most populated cluster is more considered because the resulting energy indirectly relates to binding affinity (Kozakov *et al.*, 2017). The results of the docking simulation and the structural alignment were presented in the Table 1.

Table 1. The largest clusters that represent the most likely models of the complex.

Complex	Cluster	Members	The lowest energy in the cluster*	Sequence Identity**	TM-Score**	RMSD**
RBD-Fv	1	64	-304.8	0.942	0.40	1.83
	2	54	-303.5	0.842	0.43	3.63
	3	48	-305.2	0.906	0.41	2.27
	4	42	-299.9	0.855	0.42	3.40
	5	42	-274.4	0.995	0.65	1.30
RS1-Fv	1	71	-321.4	0.898	0.41	2.53
	2	71	-282.8	0.975	0.60	2.70
	3	68	-288.3	0.920	0.41	2.42
	4	65	-307.9	0.851	0.43	2.87
	5	56	-297.9	0.777	0.45	4.01

*The energy calculated by PIPER in ClusPro

**The scores calculated by MM-Align resulted from multimeric complex alignment between the model from ClusPro and the reference complex structure (PDB ID: 7JMP)

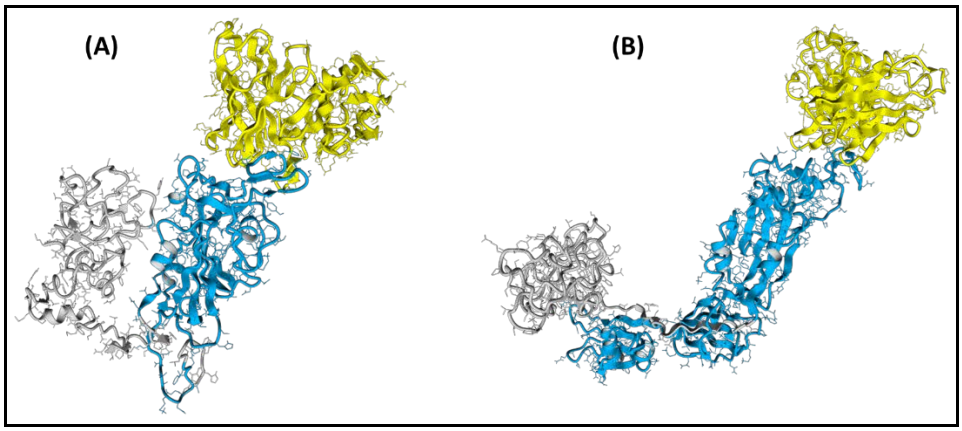

Figure 2. The structural representation of complex between antigen-TrxA fusion protein and Fv of COVA2-39 for which (A) is RBD complex and (B) is RS1 complex. The Fv is shown in yellow, the TrxA fusion protein is shown in grey, and the antigen is shown in blue.

Furthermore, the dynamic interaction between VH-VL structure and antigen-pET32b fusion was simulated in 50 ns. The complex of RBD-Fv reached its conformational stability within 3 ns with the average RMSD 10.1 Å (Figure 2A). As compared with RBD-Fv, the complex of RS1-Fv took longer time around 10 ns to maintain the stability and produced higher degree of average RMSD 13.4 Å (Figure 2B). The best complex model between antigen and antibody was chosen based on the TM-score. The complex with TM-score > 0.5 resembles the reference complex structure in terms of its global topology and chain orientation. Thus, cluster 5 with TM-score 0.65 was selected for RBD-Fv complex and cluster 2 with TM-score 0.6 was selected for RS1-Fv (Figure 2). Both selected clusters also have the highest sequence identity among other clusters, 0.995 for RBD-Fv and 0.975 for RS1-Fv. It means that the number of identical residues corresponds closely with the number of aligned residues between the model from ClusPro and the reference complex structure. The complex of RBD-Fv has lower RMSD (1.30 Å) compared to the complex of RS1-Fv (2.70 Å). Low RMSD indicates minimal local error. The RMSD or local error for both complexes is accordingly still in tolerable value.

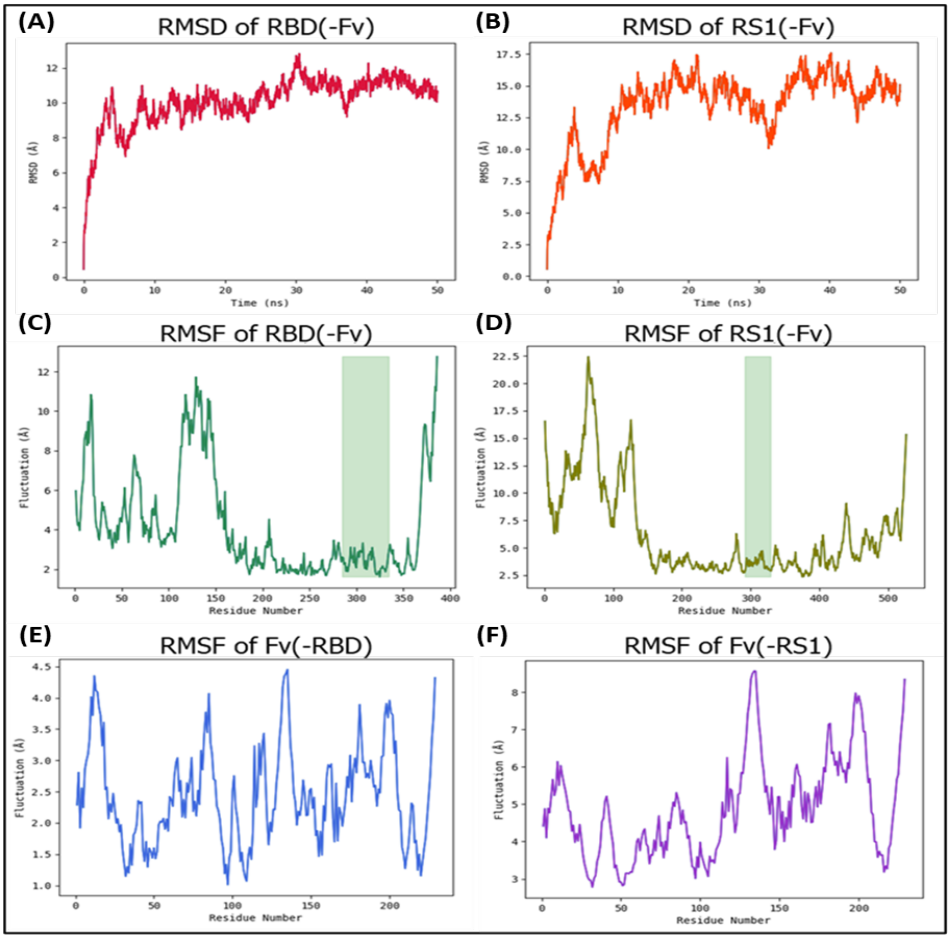

Figure 3. RMSD and RMSF analysis. RMSD of the complex: (A) RBD-Fv and (B) RS1-Fv; RMSF of the antigen: (C) RBD and (D) RS1 in complex with Fv; RMSF of the Fv in complex with antigen: (E) RBD and (F) RS1; The green boxes in (C) and (D) represent the interacting residues of the antigen with Fv.

3.3. Expression of recombinant RBD and RS1

The RBD and RS1 recombinant proteins were expressed in E. *coli* Origami strain and induced with 0.3 mM IPTG. The harvested cells were lysed and the expression of the proteins was evaluated in SDS-PAGE gels. As shown in Figure 4A, a major protein band corresponding to 45 kDa which belongs to RBD was observed in the recombinant E. *coli* after IPTG induction. Western blot was employed to evaluate the antigenicity of recombinant RBD and RS1 against antibody anti-His and polyclonal antibody anti-SARS-CoV-2 Spike RBD. Specific bands at 45 kDa and 60 kDa of RBD and RS1 recombinant protein (Figure 4B, 4C) were detected with anti-His and anti-RBD antibodies, respectively. Our results indicate that the recombinant RBD and RS1 possess the required antigenicity.

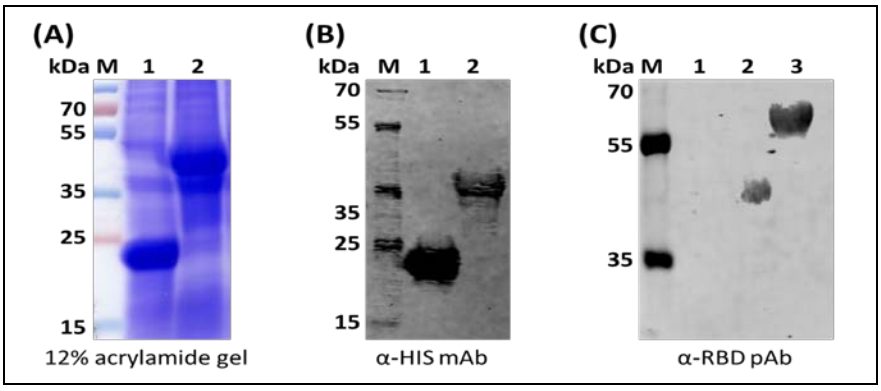

Figure 4. Expression of recombinant RBD and RS1. (a) The SDS PAGE analysis of recombinant RBD. Lane 1: induced of pET32b(+) possessing E.*coli* lysate. Lane 2: induced of pET32b(+)-RBD possessing E.*coli* lysate. (b) Reactivity of recombinant RBD probed with mouse anti-6x His tag monoclonal antibody. (c) Reactivity of recombinant RBD and RS1 with rabbit anti-SARS-CoV-2 Spike RBD pAb. Lane 1: negative control from wild-type E.*coli*. Lane 2: recombinant RBD with specific band at 45 kDa. Lane 3: recombinant RS1 with specific band at 60 kDa.

3.4. Purification of recombinant RBD and RS1 protein

To increase the production of RBD and RS1 non-classical inclusion bodies, the expression was carried out in low temperatures at 25°C, 150 rpm for 16 hours. The inclusion bodies of RBD and RS1 were solubilized using the mild denaturing buffer in 0.1 M Tris buffer 11 with a low concentration of urea 2 M, as shown in Figure 5A and 5B, respectively. Solubilization of RBD and RS1 protein from inclusion bodies was observed by increasing the pH from 8.5 to 11. Increasing urea concentration from 1 M to 2 M also improved the solubilization of the RBD and RS1 inclusion bodies. The specific band around 45 kDa and 60 kDa from RBD (blue arrow) and RS1 (red arrow) supernatant in 0.1 M tris pH 11 with 2 M urea was detected using human anti-spike monoclonal antibody in western blot analysis (Figure 5C). This result confirmed the antigenicity of solubilized RBD and RS1 with the mild buffer remains exist. Furthermore, no additional steps such as refolding were required in this study for purification. The HisTrap HP resin was employed to purify the RBD and RS1 inclusion bodies through affinity purification. As shown in Figure 5D, a major band around 45 kDa for RBD and 60 kDa for RS1 was observed upon elution with 20 mM phosphate buffer with 300 mM NaCl and 250 mM imidazole. The results indicated the recombinant RBD and RS1 were successfully produced and purified.

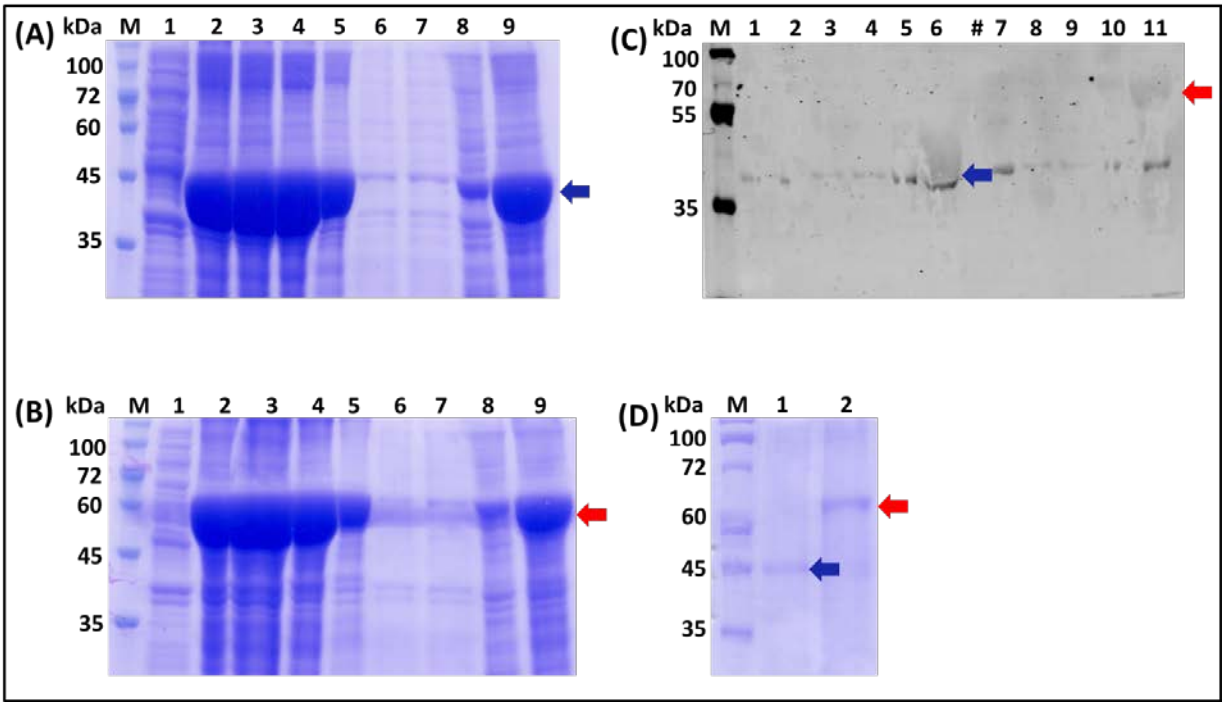

Figure 5. Isolation and purification of recombinant RBD and RS1 protein. (A,B) Effect of different lysis buffer on solubility of RBD and RS1 inclusion bodies. Lane 1: supernatant of lysed bacteria in 1X PBS buffer. Lane 2: pellet of lysed bacteria in 0.1M Tris-Cl pH 8.5 Urea 1 M. Lane 3: pellet of lysed bacteria in 0.1 M Tris-Cl pH 8.5 Urea 2 M. Lane 4: pellet of lysed bacteria in 0.1 M Tris-Cl pH 11 Urea 1 M. Lane 5: pellet of lysed bacteria in 0.1 M Tris-Cl pH 11 Urea 2 M. Lane 6: supernatant of lysed bacteria in 0.1M Tris-Cl pH 8.5 Urea 1 M. Lane 7: supernatant of lysed bacteria in 0.1 M Tris-Cl pH 8.5 Urea 2 M. Lane 8: supernatant of lysed bacteria in 0.1 M Tris-Cl pH 11 Urea 1 M. Lane 9: supernatant of lysed bacteria in 0.1 M Tris-Cl pH 11 Urea 2 M. (C) Western blot analysis of soluble inclusion bodies of RBD (lane 1-6) and RS1 (lane 7-11) detected by using human monoclonal antibody anti-spike. (D) SDS-PAGE gel of purified recombinant RBD (lane 1) and RS1 (lane 2). The recombinant RBD protein is pointed by blue arrow and the recombinant RS1 protein is pointed by red arrow.

3.5. The antigenicity evaluation of recombinant RBD and RS1 by ELISA

A total of 15 sera obtained from COVID-19 patients from different periods during the pandemic COVID-19 (2020--2022) and six naïve sera collected from pre-pandemic (2013--2015) as negative control were evaluated by indirect IgG-ELISA against recombinant RBD and RS1 (Figure 6A). No reaction was observed from all naïve pre-pandemic sera (100%) against recombinant RBD and RS1 proteins. Further, recombinant RBD reacts positively to 10 out of 15 sera (67%) according to the cut-off previously determined. Interestingly, compared to anti-RBD, recombinant RS1 protein with S1 subunit CTD appears to increase sensitivity by 80% (12 out of 15) from COVID-19 patient serum.

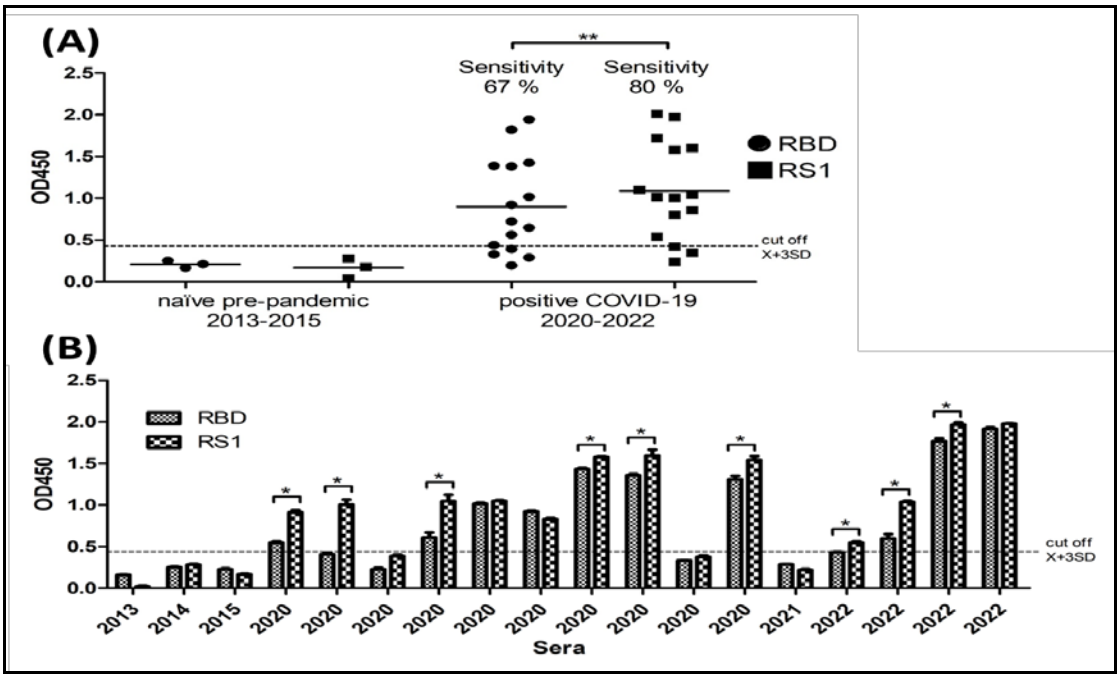

Figure 6. Evaluation of the recombinant RBD and RS1 by indirect IgG-ELISA against sera from naïve pre-pandemic and positive COVID-19. A positive sample is defined as having OD450 values of three standard deviations (SD) above the mean of a panel negative controls from naïve pre-pandemic sera. (A) The comparison sensitivity detection of RBD and RS1 was analyzed by a paired t-test. The degree of detecting antibodies anti-spike utilizing the RS1 protein increased significantly compared to RBD ($p = 0.0033$). (B) Reactivity of RBD and RS1 against antibody anti-spike from each sera is shown individually. The reactivity comparison between RBD and RS1 is statistically significant ($p<0.05$).

4. Discussion

The RBD protein is widely utilized in several applications, including serological detection and vaccine development against COVID-19 (Maffei *et al.*, 2021). Regardless of the limitation of RBD for serological detection in COVID-19, the production of the protein in the E.*coli* expression system has been reported to have several advantages over other expression systems, such as low cost and ease of handling (Ayón-Núñez *et al.*, 2022; Gao *et al.*, 2022). Additional molecules, such as streptavidin and small peptides, were exploited in E.*coli* expression system in order to enhance the solubility and functionality of RBD recombinant proteins (Brindha *et al.*, 2022; Lin *et al.*, 2023). These findings suggest that with appropriate modifications and optimizations, E.*coli*-produced RBD can achieve comparable or even improved detection sensitivity compared to mammalian expression systems. However, considering RBD mutation which affects the binding affinity and antibody escape in various "variants of concern" of SARS-CoV-2 strains (Yang *et al.*, 2021), an effort to find a new approach to increase serological detection sensitivity is needed. Evaluation of additional CTD domains in RBD recombinant to enhance the anti-spike antibody detection from COVID-19 patient sera hasn't been reported elsewhere. In this study, we constructed the recombinant plasmid encoding RBD and RBD with CTD, namely "RS1" (Figure 1A), expressed, purified, and evaluated the detection sensitivity of both constructs using a panel of COVID-19 patient sera.

In this study, several strategies were utilized in order to make our recombinant protein solubilized and refolded properly. The RBD and RS1 genes were fused with TrxA fusion protein of pET32b(+). Expression of both constructs under the TrxA fusion protein produced a larger size of recombinant RBD, as reported in the previous study (Gao *et al.*, 2022). The TrxA fusion protein promotes protein solubility and significantly reduces the formation of inclusion bodies of recombinant protein produced in E.*coli* system (Costa *et al.*, 2014). Additional strategies such as IPTG induction in low temperature and isolation with a mild denaturing buffer were utilized to enhance the solubilized inclusion bodies of RBD and RS1 protein, hence avoiding the refolding steps in purification steps.

Inclusion bodies are a common challenge encountered when using E.*coli* for recombinant protein expression (Bhatwa *et al.*, 2021). Purification of recombinant protein from inclusion bodies can be challenging. Solubilization and refolding are the critical steps to purify recombinant protein from inclusion bodies. Solubilization of inclusion bodies using a high concentration of chaotropic agent sometimes leads to protein aggregation during the refolding steps (Singh *et al.*, 2012). The expression of recombinant protein in low temperatures often results in non-classical inclusion bodies. Mild solubilization buffers could recover this type of non-classical inclusion body without losing its activity (Singh *et al.*, 2015). A certain pH of Tris buffer has been shown to make inclusion bodies of recombinant proteins produced in E.*coli* easier to dissolve (Peternel *et al.*, 2010). A previous study showed that the inclusion bodies of r-hGH were completely dissolved in a 100 mM Tris buffer with a pH of 12.5 and contained 2 M urea (Patra *et al.*, 2000).

The potency of RBD and RS1 recombinant protein to recognize anti-spike antibodies from COVID-19 patients at the acute phase was evaluated in this study. It is important to note that the construct of RBD and RS1 with CTD domain used in this study belonged to the SARS-CoV-2 Wuhan strain from the early period of COVID-19 isolated

in Indonesia. Interestingly, the RS1 recombinant protein could detect 80% (8 out of 10) and 100% (4 out of 4) antibody anti-spike from sera collected in 2020 and 2022, respectively (Figure 6B). The potency of RS1 to increase detection sensitivity is probably because of additional binding residue from CTD that could capture more anti-spike antibodies compared to RBD. The spike glycoprotein contains several epitopes directly exposed by the host immune system, making it the primary target for neutralizing antibodies (Nagesha *et al.*, 2022). A previous study documented the antibody profiles of COVID-19 patients against the full spike, NTD-S1, and CTD-S1 antigens, highlighting their dynamic nature. Over 90% of the patients recovering from COVID-19 showed immune responses, specifically IgG and IgM, that targeted the CTD-S1 antigen. These responses were similar to those observed for the full spike. Meanwhile, a mere 3.33% of the recovered patients showed IgG reactivity to NTD-S1 (Bao *et al.*, 2021). In accordance with the previous report (Bao *et al.*, 2021), the addition of CTD domain in our RBD construct (RS1) significantly increases the sensitivity of the serological assay of anti-spike antibodies compared to RBD ($p = 0.0033$). Furthermore, the SARS-CoV-2 S1 subunit CTD binding interface has more residues that directly interact with the receptor ACE2 than does SARS-S1 RBD (Huang *et al.*, 2020). The size of an antigen can affect the immune response in humans and induce more humoral immune response (Heida *et al.*, 2022; Zinkhan *et al.*, 2021). In this sense, the circulated anti-spike antibodies are not limited to RBD domain, but also another area such as CTD of S1 domain. Considering the abundance and variety of antibodies, it is conceivable to develop the ELISA assay harboring RBD with an additional CTD domain to increase the monitoring sensitivity of the spike antibody in the population.

Based on the RBD and RS1 modeling structure from the in silico study, RS1 structure (Figure 2B) showed a greater protein surface that could elicit more antigenic antibody determinants. It is correlated with the ELISA result of RS1, which had higher detection sensitivity. From the molecular dynamics result, the different topologies of RBD-Fv and RS1-Fv complexes may cause RMSD differences, especially the longer chain of the RS1 that makes the pET32b open out (Figure 2B). The extended RBD chain in RS1 seems like a linker region between RBD chain and pET32b(+) that lead to the open conformation. This open conformation gives rise to the greater fluctuation of amino acid residues during dynamic simulation and, consequently, the backbones deviate more from its original state. The first 150 residues are the pET32b part that accounts for the greatest fluctuations of the overall antigen molecule (Figure 3C and 3D). On the other hand, residue fluctuation in Fv molecule binding to RBD has almost the same pattern as Fv molecule binding to RS1 (Figure 3E and 3F). The higher fluctuations occur mostly in the loop regions, which are more flexible and undergo random motions, especially those in the surface area. The binding stability between antigen and antibody can be seen through RMSF of the interacting residues (Figure 3C and 3D). Major residues in the contact region generate Van der Waals interaction. Some others use pi-pi stacks and hydrogen bonds. These interactions increase the binding affinity and stabilize the binding between antigen and antibody, leading to low fluctuations in the interacting residues. The average RMSF of interacting residues in RBD is lower (2.0 Å) than that of RS1 (3.3 Å). Compared with RBD, RS1 produced a two-fold higher degree of fluctuation in the overall complex due to its open conformation. Due to the different topology of modeled structure between RBD and RS1, we cannot conclude that the system's lower fluctuations of RBD amino acid residues correspond to higher binding affinity with the antibody molecule. Mainly because the interacting residues with the antibody in both RBD and RS1 show relatively low fluctuation, both antigens have stable binding with the antibody. The epitope antigenicity between RBD and RS1 should be compared for further study.

5. Conclusion

Antigen size affects the immune response in humans, specifically the humoral immune response. In this sense, the circulated anti-spike antibodies are not limited to targeting the RBD domain but also targeting another area, such as the C terminal domain (CTD). Considering the abundance and variety of antibodies, developing the ELISA assay harboring RBD with an additional CTD domain is conceivable to increase the monitoring sensitivity of the relevant antibody in the population.

Acknowledgments

This research was supported by the DIPA grant 2021 Menristek/BRIN and RIIM grant (B-3451/II.7.5/FR.06.00/10/2023), BRIN.

Competing Interests

The authors declare no competing interests.

References

Ayón-Núñez, D. A., Cervantes-Torres, J., Cabello-Gutiérrez, C., Rosales-Mendoza, S., Rios-Valencia, D., Huerta, L., Bobes, R. J., Carrero, J. C., Segura-Velázquez, R., Fierro, N. A., Hernández, M., Zúñiga-Ramos, J., Gamba, G., Cárdenas, G., Frías-Jiménez, E., Herrera, L. A., Fragoso, G., Sciutto, E., Suárez-Güemes, F., & Laclette, J. P. (2022). An RBD-Based Diagnostic Method Useful for the Surveillance of Protective Immunity against SARS-CoV-2 in the Population. *Diagnostics (Basel)*, **12**. doi:10.3390/diagnostics12071629

Bao, Y., Ling, Y., Chen, Y. Y., Tian, D., Zhao, G. P., Zhang, X. H., Hang, H., Li, Y., Su, B., Lu, H. Z., Xu, J., & Wang, Y. (2021). Dynamic anti-spike protein antibody profiles in COVID-19 patients. *Int J Infect Dis*, **103**:540-548. doi:10.1016/j.ijid.2020.12.014

Bhatwa, A., Wang, W., Hassan, Y. I., Abraham, N., Li, X. Z., & Zhou, T. (2021). Challenges Associated With the Formation of Recombinant Protein Inclusion Bodies in Escherichia coli and Strategies to Address Them for Industrial Applications. *Front Bioeng Biotechnol*, **9**:630551. doi:10.3389/fbioe.2021.630551

Biswas, S., Mahmud, S., Mita, M. A., Afrose, S., Hasan, M. R., Sultana Shimu, M. S., Saleh, M. A., Mostafa-Hedeab, G., Alqarni, M., Obaidullah, A. J., & Batiha, G. E. (2021). Molecular Docking and Dynamics Studies to Explore Effective Inhibitory Peptides Against the Spike Receptor Binding Domain of SARS-CoV-2. *Front Mol Biosci*, **8**:791642. doi:10.3389/fmolb.2021.791642

Brenke, R., Hall, D. R., Chuang, G.-Y., Comeau, S. R., Bohnuud, T., Beglov, D., Schueler-Furman, O., Vajda, S., & Kozakov, D. (2012). Application of asymmetric statistical potentials to antibody–protein docking. *Bioinformatics*, **28**: 2608-2614. doi:10.1093/bioinformatics/bts493

Brindha, S., & Kuroda, Y. (2022). A Multi-Disulfide Receptor-Binding Domain (RBD) of the SARS-CoV-2 Spike Protein Expressed in E. coli Using a SEP-Tag Produces Antisera Interacting with the Mammalian Cell Expressed Spike (S1) Protein. *Int J Mol Sci*, **23**. doi:10.3390/ijms23031703

Brouwer, P. J. M., Caniels, T. G., van der Straten, K., Snitselaar, J. L., Aldon, Y., Bangaru, S., Torres, J. L., Okba, N. M. A., Claireaux, M., Kerster, G., Bentlage, A. E. H., van Haaren, M. M., Guerra, D., Burger, J. A., Schermer, E. E., Verheul, K. D., van der Velde, N., van der Kooi, A., van Schooten, J., van Breemen, M. J., Bijl, T. P. L., Sliepen, K., Aartse, A., Derking, R., Bontjer, I., Kootstra, N. A., Wiersinga, W. J., Vidarsson, G., Haagmans, B. L., Ward, A. B., de Bree, G. J., Sanders, R. W., & van Gils, M. J. (2020). Potent neutralizing antibodies from COVID-19 patients define multiple targets of vulnerability. *Science*, 369:643-650. doi:10.1126/science.abc5902

Costa, S., Almeida, A., Castro, A., & Domingues, L. (2014). Fusion tags for protein solubility, purification and immunogenicity in Escherichia coli: the novel Fh8 system. *Front Microbiol*, **5**. doi:10.3389/fmicb.2014.00063

Fraser, D. D., Miller, M. R., Martin, C. M., Slessarev, M., Hahn, P., Higgins, I., Melo, C., Pest, M. A., Rothery, N., Wang, X., Zeidler, J., & Cruz-Aguado, J. A. (2022). Cohort-Specific Serological Recognition of SARS-CoV-2 Variant RBD Antigens. *Ann Clin Lab Sci*, **52**:651-662.

Gao, X., Peng, S., Mei, S., Liang, K., Khan, M. S. I., Vong, E. G., & Zhan, J. (2022). Expression and functional identification of recombinant SARS-CoV-2 receptor binding domain (RBD) from E. coli system. *Prep Biochem Biotechnol*, **52**:318-324. doi:10.1080/10826068.2021.1941106

He, Y., Qi, J., Xiao, L., Shen, L., Yu, W., & Hu, T. (2021). Purification and characterization of the receptor-binding domain of SARS-CoV-2 spike protein from Escherichia coli. *Eng Life Sci*, **21**:453-460. doi:10.1002/elsc.202000106

Heida, R., Born, P. A., Tapia-Calle, G., Frijlink, H. W., Salvati, A., Huckriede, A. L. W., & Hinrichs, W. L. J. (2022). Assessing the Immunomodulatory Effect of Size on the Uptake and Immunogenicity of Influenza- and Hepatitis B Subunit Vaccines In Vitro. *Pharmaceuticals (Basel)*, **15**. doi:10.3390/ph15070887

Huang, Y., Yang, C., Xu, X.-f., Xu, W., & Liu, S.-w. (2020). Structural and functional properties of SARS-CoV-2 spike protein: potential antivirus drug development for COVID-19. *Acta Pharmacol. Sin.*, **41**:1141-1149. doi:10.1038/s41401-020-0485-4

Kozakov, D., Hall, D. R., Xia, B., Porter, K. A., Padhorny, D., Yueh, C., Beglov, D., & Vajda, S. (2017). The ClusPro web server for protein-protein docking. *Nat. Protoc.*, **12**:255-278. doi:10.1038/nprot.2016.169

Krähling, V., Halwe, S., Rohde, C., Becker, D., Berghöfer, S., Dahlke, C., Eickmann, M., Ercanoglu, M. S., Gieselmann, L., Herwig, A., Kupke, A., Müller, H., Neubauer-Rädel, P., Klein, F., Keller, C., & Becker, S. (2021). Development and characterization of an indirect ELISA to detect SARS-CoV-2 spike protein-specific antibodies. *J Immunol Methods*, **490**. 112958. doi:10.1016/j.jim.2021.112958

Krieger, E., & Vriend, G. (2014). YASARA View - molecular graphics for all devices - from smartphones to workstations. *Bioinformatics*, **30**:2981-2982. doi:10.1093/bioinformatics/btu426

Lee, J., Cheng, X., Swails, J. M., Yeom, M. S., Eastman, P. K., Lemkul, J. A., Wei, S., Buckner, J., Jeong, J. C., Qi, Y., Jo, S., Pande, V. S., Case, D. A., Brooks, C. L., III, MacKerell, A. D., Jr., Klauda, J. B., & Im, W. (2016). CHARMM-GUI Input Generator for NAMD, GROMACS, AMBER, OpenMM, and CHARMM/OpenMM Simulations Using the CHARMM36 Additive Force Field. *J. Chem. Theory Comput.*, **12**:405-413. doi:10.1021/acs.jctc.5b00935

Lin, W.-Z., Wang, J.-P., Ma, I. C., Hsieh, P.-C., Hung, Y.-J., Hung, C.-M., & Hou, S.-Y. (2023). Highly sensitive β-galactosidase detection using streptavidin-display E. coli and lateral flow immunoassay. *Sens. Actuators, A.*, **350**. 114114. doi:https://doi.org/10.1016/j.sna.2022.114114

Liu, L., Jiao, Y., Yang, M., Wu, L., Long, G., & Hu, W. (2023). Network Pharmacology, Molecular Docking and Molecular Dynamics to Explore the Potential Immunomodulatory Mechanisms of Deer Antler. *Int J Mol Sci*, **24**. doi:10.3390/ijms241210370

Maffei, M., Montemiglio, L. C., Vitagliano, G., Fedele, L., Sellathurai, S., Bucci, F., Compagnone, M., Chiarini, V., Exertier, C., Muzi, A., Roscilli, G., Vallone, B., & Marra, E. (2021). The Nuts and Bolts of SARS-CoV-2 Spike Receptor-Binding Domain Heterologous Expression. *Biomolecules*, **11**. doi:10.3390/biom11121812

Mukherjee, S., & Zhang, Y. (2009). MM-align: a quick algorithm for aligning multiple-chain protein complex structures using iterative dynamic programming. *Nucleic Acids Res*, **37**. e83. doi:10.1093/nar/gkp318

Nagesha, S. N., Ramesh, B. N., Pradeep, C., Shashidhara, K. S., Ramakrishnappa, T., Bagoji, M., & Chandaragi, S. S. (2022). SARS-CoV 2 spike protein S1 subunit as an ideal target for stable vaccines: A bioinformatic study. *Mater Today Proc*, **49**:904-912. doi:10.1016/j.matpr.2021.07.163

Oglat, A. A., Oqlat, M. A., Oqlat, A. A., Alanagreh, L. a., Khaniabadi, P. M., Dheyab, M. A., Khaleel, H., & Althalji, O. (2022). Imaging Aspects (Chest Radiographic and CT Scan Findings) of COVID-19 with Clinical Classifications. *Jordan J Biol Sci.*, **15**.

Patra, A. K., Mukhopadhyay, R., Mukhija, R., Krishnan, A., Garg, L. C., & Panda, A. K. (2000). Optimization of inclusion body solubilization and renaturation of recombinant human growth hormone from Escherichia coli. *Protein Expr Purif*, **18**:182-192. doi:10.1006/prep.1999.1179

Peterhoff, D., Glück, V., Vogel, M., Schuster, P., Schütz, A., Neubert, P., Albert, V., Frisch, S., Kiessling, M., Pervan, P., Werner, M., Ritter, N., Babl, L., Deichner, M., Hanses, F., Lubnow, M., Müller, T., Lunz, D., Hitzenbichler, F., Audebert, F., Hähnel, V., Offner, R., Müller, M., Schmid, S., Burkhardt, R., Glück, T., Koller, M., Niller, H. H., Graf, B., Salzberger, B., Wenzel, J. J., Jantsch, J., Gessner, A., Schmidt, B., & Wagner, R. (2021). A highly specific and sensitive serological assay detects SARS-CoV-2 antibody levels in COVID-19 patients that correlate with neutralization. *Infection*, **49**:75-82. doi:10.1007/s15010-020-01503-7

Peternel, S., & Komel, R. (2010). Isolation of biologically active nanomaterial (inclusion bodies) from bacterial cells. *Microb Cell Fact*, **9**. doi:10.1186/1475-2859-9-66

Piovesan, D., Minervini, G., & Tosatto, S. C. (2016). The RING 2.0 web server for high quality residue interaction networks. *Nucleic Acids Res*, **44**:W367-374. doi:10.1093/nar/gkw315

Rastogi, Y. R., Sharma, A., Nagraik, R., Aygün, A., & Şen, F. (2020). The novel coronavirus 2019-nCoV: Its evolution and transmission into humans causing global COVID-19 pandemic. *Int J Environ Sci Technol (Tehran)*, **17**:4381-4388. doi:10.1007/s13762-020-02781-2

Shwan, N. A., Aziz, S. S., Hamad, B. K., & Hussein, O. A. (2022). Characterizing New Genomic and Proteomic Variations among SARS-CoV-2 Strains. *Jordan J Biol Sci.*, **15**.

Singh, A., Upadhyay, V., Upadhyay, A. K., Singh, S. M., & Panda, A. K. (2015). Protein recovery from inclusion bodies of Escherichia coli using mild solubilization process. *Microb Cell Fact*, **14**. doi:10.1186/s12934-015-0222-8

Singh, S. M., Sharma, A., Upadhyay, A. K., Singh, A., Garg, L. C., & Panda, A. K. (2012). Solubilization of inclusion body proteins using n-propanol and its refolding into bioactive form. *Protein Expr Purif.*, **81**:75-82. doi:https://doi.org/10.1016/j.pep.2011.09.004

Tai, W., He, L., Zhang, X., Pu, J., Voronin, D., Jiang, S., Zhou, Y., & Du, L. (2020). Characterization of the receptor-binding domain (RBD) of 2019 novel coronavirus: implication for development of RBD protein as a viral attachment inhibitor and vaccine. *Cell. Mol. Immunol.*, **17**:613-620. doi:10.1038/s41423-020-0400-4

Wu, N. C., Yuan, M., Liu, H., Lee, C. D., Zhu, X., Bangaru, S., Torres, J. L., Caniels, T. G., Brouwer, P. J. M., van Gils, M. J., Sanders, R. W., Ward, A. B., & Wilson, I. A. (2020). An Alternative Binding Mode of IGHV3-53 Antibodies to the SARS-CoV-2 Receptor Binding Domain. *Cell Rep*, **33**.108274. doi:10.1016/j.celrep.2020.108274

Xu, J., & Zhang, Y. (2010). How significant is a protein structure similarity with TM-score = 0.5? *Bioinformatics*, **26**:889-895. doi:10.1093/bioinformatics/btq066

Yang, J., Yan, R., Roy, A., Xu, D., Poisson, J., & Zhang, Y. (2015). The I-TASSER Suite: protein structure and function prediction. *Nat. Methods*, **12**:7-8. doi:10.1038/nmeth.3213

Yang, L., Li, J., Guo, S., Hou, C., Liao, C., Shi, L., Ma, X., Jiang, S., Zheng, B., Fang, Y., Ye, L., & He, X. (2021). SARS-CoV-2 Variants, RBD Mutations, Binding Affinity, and Antibody Escape. *Int J Mol Sci*, **22**. doi:10.3390/ijms222212114

Yin, Q., Zhang, Y., Lian, L., Qu, Y., Wu, W., Chen, Z., Pei, R., Chen, T., Sun, L., Li, C., Li, A., Li, J., Li, D., Wang, S., Guan, W., & Liang, M. (2021). Chemiluminescence Immunoassay Based Serological Immunoassays for Detection of SARS-CoV-2 Neutralizing Antibodies in COVID-19 Convalescent Patients and Vaccinated Population. *Viruses*, **13**. doi:10.3390/v13081508

Zinkhan, S., Ogrina, A., Balke, I., Reseviča, G., Zeltins, A., de Brot, S., Lipp, C., Chang, X., Zha, L., Vogel, M., Bachmann, M. F., & Mohsen, M. O. (2021). The impact of size on particle drainage dynamics and antibody response. *J Control Release*, *331*, 296-308. doi:10.1016/j.jconrel.2021.01.012